Equipartition theorem and the dynamics of liquids

V. A. Levashov
Department of Physics and Astronomy, University of Tennessee, Knoxville, Tennessee 37996, USA

T. Egami
Department of Physics and Astronomy, and Department of Materials Science and Engineering, University of Tennessee, Knoxville, Tennessee 37996, USA,
and Oak Ridge National Laboratory, Oak Ridge, Tennessee 37831, USA

R. S. Aga
Materials Science and Technology Division, Oak Ridge National Laboratory, Oak Ridge, Tennessee 37831, USA

J. R. Morris
Materials Science and Technology Division, Oak Ridge National Laboratory, Oak Ridge, Tennessee 37831-6115, USA,
and Department of Materials Science and Engineering, University of Tennessee, Knoxville, Tennessee 37996-2200, USA
(Received 5 May 2008; revised manuscript received 14 July 2008; published 21 August 2008)

In liquids, phonons have a very short lifetime and the total potential energy does not depend linearly on temperature. Thus it may appear that atomic vibrations in liquids cannot be described by the harmonic-oscillator model and that the equipartition theorem for the potential energy is not upheld. In this paper we show that the description of the local atomic dynamics in terms of the atomic-level stresses provides such a description, satisfying the equipartition theorem. To prove this point we carried out molecular-dynamics simulations with several pairwise potentials, including the Lennard-Jones potential, the modified Johnson potential, and the repulsive part of the Johnson potential, at various particle number densities. In all cases studied the total self-energy of the atomic-level stresses followed the $(3/2)k_BT$ law. From these results we suggest that the concept of local atomic stresses can provide description of thermodynamic properties of glasses and liquids on the basis of harmonic atomistic excitations. An example of application of this approach to the description of the glass transition temperature in metallic glasses is discussed.

DOI: 10.1103/PhysRevB.78.064205 PACS number(s): 61.20.Ne, 61.20.Ja, 61.43.Fs

I. INTRODUCTION

The lattice dynamics of crystals can be described well in terms of phonons because of the periodicity of the lattice. In liquids and glasses, however, in the absence of the lattice periodicity, phonons are scattered strongly except for very long wavelengths. Furthermore, the potential energy of liquids generally does not depend linearly on temperature. Instead it could be often fitted with the Rosenfeld-Tarazona $(-U_o+aT^{3/5})$ formula[1,2] that was justified with the use of the density-functional theory.[1] Thus it may appear that it is impossible to introduce the description of the dynamics of liquids and glasses in terms of the harmonic-oscillator model.

A major reason for this difficulty is that the structure of a liquid is temperature dependent and a part of the temperature dependence of the total potential energy originates from the temperature-dependent configurational energy. Then it may be possible that the vibrational part of the energy can be described in terms of the harmonic excitation models while the temperature dependence of the configurational energy could be expressed separately, for instance, in terms of the energy of the inherent structure of the potential-energy landscape (PEL) theory.[3–5] However, vibrational modes in the liquid have a very short lifetime, i.e., of the order of 10^{-13} s, with many of them having imaginary frequencies, making the analysis of atomic dynamics difficult.[6,7]

Earlier we made an attempt to describe the liquid structure, energetics, and dynamics with a rather different approach. The concept of atomic-level stresses was introduced to characterize the distortions of the local atomic environment from an ideal state.[8–13] It was then demonstrated that the total self-energy of the atomic-level stresses follows the simple equipartition $(3/2)k_BT$ law at temperatures well above the glass transition temperature. Moreover, this total self-energy is equipartitioned among the six stress components, i.e., one compression/dilation component and five shear components.[13] This means that the dynamics of the atomic-level stresses may approximately describe the atomic dynamics in the system and could be used as the basis for the statistical mechanics of liquids.

The earlier demonstration, however, was made only for the short-range modified Johnson pair potential (mJp) developed for iron. In this paper we show that the equipartition theorem is more generally applicable by testing it for several different pair potentials. The potentials we have chosen are the Lennard-Jones potential, the modified Johnson potential, and finally, motivated by the idea that, to a large extent, liquid structures are determined by the repulsive part of the potential,[14] we also made simulations retaining only the repulsive part of the modified Johnson pair potential. The calculations were performed at various number densities. We found that in all cases stress self-energies follow the $(3/2)k_BT$ law extremely well.

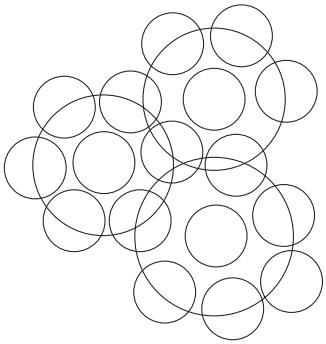

FIG. 1. Schematic of the nearest-neighbor shells.

II. ATOMIC LEVEL STRESSES

The concept of atomic-level stresses was introduced earlier to describe the local structure of metallic glasses.[8–13] In order to gain intuitive understanding of the atomic-level stresses, it is useful to consider packing of soft spheres. Imagine that a soft sphere is confined in the cage formed by its nearest neighbors (see Fig. 1). If this cage is smaller than the size of the central sphere itself, then the sphere at the center of the cage is under compression. On the other hand if the cage is larger, the central sphere is under dilation. Furthermore the cage may not be spherical in shape. In this case the central sphere experiences shear stresses. Thus, the atomic-level stresses describe the topology and geometry of the nearest neighbors.

Let us suppose that we consider an assembly of atoms interacting via a pairwise potential, $\phi(r)$. If this system is distorted by an infinitesimal homogeneous strain tensor ϵ^{ab}, the change in its potential energy could be written as[12]

$$\Delta E = \frac{1}{2}\sum_{ij} \Delta E_{ij} = \sum_{i} \Delta E_1(i) + \sum_{i} \Delta E_2(i) \ldots , \tag{1}$$

where

$$\Delta E_1(i) = \sum_{ab} V_i \sigma_i^{ab} \epsilon^{ab}, \tag{2}$$

and

$$\Delta E_2(i) = \frac{1}{2}\sum_{abcd} V_i C_i^{abcd} \epsilon^{ab} \epsilon^{cd}. \tag{3}$$

V_i, σ_i^{ab}, and C_i^{abcd} are the atomic volume, the atomic-level stress, and the atomic-level elastic modulus of the atom i. The summations over i and j are over all atoms in the system, and the summations over a, b, c, and d are over Cartesian components. The expression for local atomic-level stresses σ_i^{ab} from potential-energy expansion is the following (neglecting the kinetic-energy contribution, which is trivial and separable for classical systems):

$$\sigma_i^{ab} = \frac{1}{2V_i}\sum_{j} \left[\frac{d\phi(r_{ij})}{dr_{ij}}\right] r_{ij} \left(\frac{r_{ij}^a r_{ij}^b}{r_{ij}^2}\right), \tag{4}$$

where r_{ij} is the distance between atoms i and j, $r_{ij}=|\vec{r}_j-\vec{r}_i|$. The expressions for the local atomic elastic constants could be found in Ref. 12. A sensible way to define local atomic volume V_i in Eqs. (2)–(4) is to use Voronoi polyhedra. However, for the sake of simplicity, we used an essentially equivalent but simpler approach, calculating V_i using a weighted average near-neighbor distance for atom i, adopted earlier[9] (see also Appendix B).

Since liquids and glasses are macroscopically isotropic, it is natural to use the spherical representation of the stresses or equivalently the cubic representation.[12] The stress components in the cubic representation are:

$$\sigma_i^{\alpha} = \sqrt{\frac{1}{3}}[\sigma_i^{xx} + \sigma_i^{yy} + \sigma_i^{zz}], \tag{5}$$

$$\sigma_i^{\gamma_1} = \sqrt{\frac{2}{3}}\left[\sigma_i^{zz} - \frac{1}{2}(\sigma_i^{yy} + \sigma_i^{zz})\right], \tag{6}$$

$$\sigma_i^{\gamma_2} = \sqrt{\frac{1}{2}}[\sigma_i^{xx} - \sigma_i^{yy}], \quad \sigma_i^{\epsilon_1} = \sqrt{2}\sigma_i^{yz}, \tag{7}$$

and

$$\sigma_i^{\epsilon_2} = \sqrt{2}\sigma_i^{zx}, \quad \sigma_i^{\epsilon_3} = \sqrt{2}\sigma_i^{xy}. \tag{8}$$

Here σ^{α} corresponds to the atomic-level pressure,

$$P_i = \left(\frac{1}{\sqrt{3}}\right)\sigma_i^{\alpha}, \tag{9}$$

while the other five atomic-level stresses represent shear stresses that are macroscopically equivalent to each other and describe the shear deformation of local atomic environment.

Equations (2) and (3) could also be expressed in the cubic representation:

$$\Delta E_1(i) = V_i \sum_{\omega} \sigma_i^{\omega} \epsilon^{\omega}, \tag{10}$$

and

$$\Delta E_2(i) = \frac{1}{2} V_i \sum_{\omega} C_i^{\omega} (\epsilon^{\omega})^2 + \ldots , \tag{11}$$

where the superscript ω marks the components of the stresses, strains, and elastic constants in the cubic representation. The off-diagonal terms in Eq. (11) vanish for a perfectly isotropic system.

III. SELF-ENERGY OF ATOMIC LEVEL STRESSES

We now calculate the local elastic energy associated with the atomic-level stresses. For this purpose we consider an idealized amorphous state. We assume that in such a state all the nearest-neighbor atoms are at the ideal distance from each other, corresponding to the minimum in the interatomic potential. Thus all the atomic-level stresses are zero in a nearest-neighbor approximation. In this state the first term in Eq. (1) is zero. Furthermore we assume that the local elastic constants are spatially uniform in the mean-field approximation and use the spatial averages of the model that depend on temperature. Thus Eq. (11) is now

$$\Delta E_2(i) = \frac{1}{2}\langle V_i\rangle \sum_{\omega} \langle C_i^{\omega}\rangle (\epsilon^{\omega})^2 + \ldots \tag{12}$$

We then recover the original glass structure by locally deforming the ideal structure. We assume that the local strain necessary to do this is given by

$$\epsilon_i^{\omega} \equiv \frac{\sigma_i^{\omega}}{\langle C_i^{\omega}\rangle}. \tag{13}$$

Equation (12) is now

$$\Delta E_2(i) = \langle V_i\rangle \sum_{\omega} \frac{\langle C_i^{\omega}\rangle}{2}\left(\frac{\sigma_i^{\omega}}{\langle C_i^{\omega}\rangle}\right)^2. \tag{14}$$

The averaging of Eq. (14) over all sites (or over time for a single site) leads to the expression for the self-energy of the atomic-level stresses,

$$\langle \Delta E\rangle = \sum_{\omega} \frac{\langle V_i\rangle \langle (\sigma_i^{\omega})^2\rangle}{2\langle C_i^{\omega}\rangle}. \tag{15}$$

When the average stress, which is equal to the external stress, is not zero, as is in some cases described below, the ideal state should be defined as the state that has the atomic-level stress equal to the average everywhere. Thus the self-energy of the ω component of the stresses is

$$\langle \Delta E^{\omega}\rangle = \frac{\langle V_i\rangle \langle (\sigma_i^{\omega} - \langle \sigma_i^{\omega}\rangle)^2\rangle}{2\langle C_i^{\omega}\rangle}. \tag{16}$$

The assumption of independent oscillators leads to the standard result for harmonic system, i.e., the average energies of the different stress components should be equal to each other. Since the total potential energy of $(3/2)k_BT$ is equally divided among the six components, it is natural to expect that the ensemble average of the energy for every stress component will lead to

$$\langle \Delta E^{\omega}(i)\rangle = \left(\frac{1}{6}\right)\left(\frac{3}{2}\right)k_BT = \frac{1}{4}k_BT, \tag{17}$$

for all stress components. This result was indeed confirmed by Chen *et al.* in Ref. 13 and it is reproduced below.

Equipartition of the potential energy among different shear components is expected since they are macroscopically equivalent to each other. However the fact that the pressure component of the self-energy is equal to the self-energy of the shear stresses is, from our point of view, quite nontrivial. Since the atomic-level stresses primarily depend on the relative position of the nearest neighbors, Eq. (17) means that the dynamics of the nearest-neighbor shell fluctuations (Fig. 1) is approximately harmonic and independent from each other at high temperatures.

In deriving Eq. (16), we assumed that all stress components on all sites (and on the same site) are totally independent from each other. Thus the local strains do not satisfy the static compatibility condition. This should apply only at temperatures high enough not to have atomic correlations.

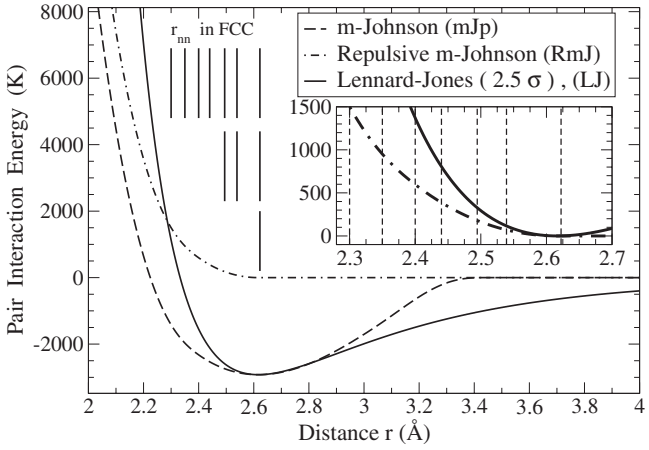

FIG. 2. Pair potentials used in MD simulations. For the repulsive part of the modified Johnson potential, simulations were performed at seven different number densities. If the system at these densities would form fcc lattice then the distances between the nearest neighbors would correspond to the positions of the seven top bars in the main plot. For the Lennard-Jones potential, simulations were performed at three different densities that correspond to the three middle bars. For the full modified Johnson potential, simulations were performed at a density that corresponds to the minimum of the potential.

The average values of the elastic constant are related to the instantaneous, or high frequency, bulk B and shear G moduli of the material via

$$B = \frac{1}{3}\langle C_i^{\alpha}\rangle, \quad G = \frac{1}{2}\langle C_i^{\gamma_1}\rangle. \tag{18}$$

The distributions of the atomic-level elastic constants for the Lennard-Jones potential are shown in Appendix B.

IV. DETAILS OF MOLECULAR-DYNAMICS SIMULATIONS

In our molecular-dynamics (MD) simulations, we studied single-component systems of particles interacting through the three different pairwise potentials shown in Fig. 2. The simulations were performed on the systems consisting of 5488 particles with the mass of iron. The time step was chosen to be 10^{-15} s. In each case the total volume was kept constant. The periodic boundary conditions were applied. A fifth-order Gear algorithm was used to integrate equations of motion.[15]

We started with the mJp described in Appendix A.[16,17] We also considered the repulsive part of the modified Johnson pair potential (RmJ) that was obtained by using a cutoff at the minimum of the mJp and by shifting the repulsive part to zero at the cutoff distances. Lastly we used the Lennard-Jones (LJ) potential that was cut and shifted at 2.5σ. We choose the parameters of the LJ potential in such a way that the minimum of the cut and shifted potential matches the position and depth of the mJp, as described in Appendix A.

Simulations with the RmJ were done for seven different fixed densities. The distances between the nearest neighbors

TABLE I. Densities and crystallization temperatures.

$r_{nn}(fcc)$ (Å)	ρ 10^{-2} (Å^{-3})	$T_{\min}$(LJ) (K)	$T_{\min}$(mJp) (K)	$T_{\min}$(RmJ) (K)
2.6223	7.843	2200	1300	650
2.5391	8.640	3700		1100
2.4945	9.111	4800		1600
2.4400	9.735			2100
2.4000	10.230			2500
2.3500	10.897			3200
2.3000	11.623			3800

in the fcc lattice at these densities, ($\rho=\sqrt{2}/r_{nn}^3$), are shown as vertical bars (top seven bars) in Fig. 2 (see also Table I). Simulations on the LJ potential were done for three different densities that are also shown as vertical bars (three middle bars) in Fig. 2. Simulations on the full mJp were done only for one density $\rho_o=0.07843$ Å^{-3} in order to verify the previous results.[13]

Temperature was introduced using simple temperature rescaling algorithm.[18,19] Thus we averaged the kinetic energy of the particles over the ensemble and over some time window (10^5 MD steps). The average value of the kinetic energy over the time window, in general, deviates from the target value of the average kinetic energy that corresponds to the target temperature. Thus at the end of the time window, we rescaled the velocity of particles according to $\vec{v}_i' = \vec{v}_i\sqrt{K_{\text{tar}}/K_{\text{ave}}}$, where $K_{\text{tar}}=(3/2)k_BT$ is the target value of average kinetic energy and K_{ave} is the average value of the kinetic energy over the time window.

In order to obtain a liquid state, we started simulations on the bcc lattice at low densities ($r_{nn}=3.54$ Å) and at high temperatures (10 000 K). After some time (10^5 MD steps), the system melted and equilibrated. Then we rescaled the coordinates of particles to the required density and instantaneously (quench) reduced the temperature using velocity rescaling. The relaxation of the system was controlled using the time dependence of potential energy per particle and the pair-density function (PDF).

Since we studied single-component systems, our liquids tended to crystallize at temperatures near the glass transition temperature. However, in this work we are interested in testing the equipartition theorem for stable liquids at higher temperatures. Thus we were not concerned with the behavior of the system near the glass transition. The lowest studied temperatures for which crystallization does not occur for a time sufficient to collect statistics (10^6 MD steps) for every potential and density studied are presented in Table I. The highest studied temperature was chosen to be 5000 K for all potentials and densities. For each temperature studied, we selected 100 structures with 10 000 MD steps between the consequent structures for the data analysis.

V. RESULTS

Figure 3 shows the PDF for some of the studied potentials and densities at temperatures just above the crystallization

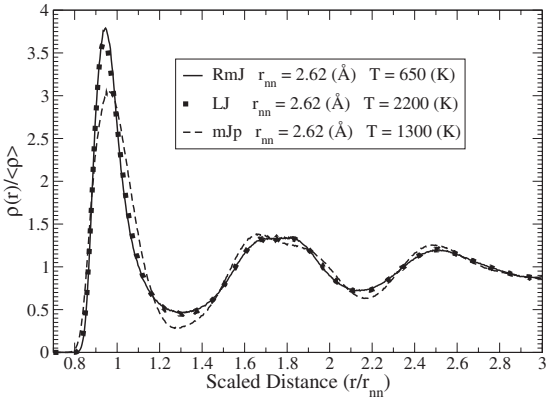

FIG. 3. Scaled radial pair-density functions for some of the studied systems. All the curves shown are for temperatures just above the crystallization temperature.

temperature. It is interesting to note that the results from the RmJ and those from the LJ potentials essentially coincide beyond the first peak. This is probably because the LJ potential is strongly anharmonic and is dominated by the repulsive core of the potential. The result from the full mJp is somewhat different. In particular the minimum in the PDF beyond the first peak is better defined. The mJp has a region with a strongly negative curvature in the vicinity of the minimum in the PDF. This promotes clearer bifurcation of the nearest and second-nearest neighbors, resulting in the deeper minimum in the PDF. In all cases the first minimum of the pair-density function is relatively well defined. This allows us to define the nearest neighbors and the first coordination shell—the concepts that are essential for the derivation of formulas in Secs. II and III.

The local atomic volume, local atomic-level stresses, and local atomic elastic constants were calculated from particle coordinates. The distributions for some of these parameters are shown in Appendix B. Thus we calculate the average values of all parameters and the mean-square deviations of local atomic stresses, and obtain the stress self-energies.

Figure 4 shows the temperature dependence of the stress self-energies [Eq. (16)] from the simulations using the LJ potential for three different densities. In calculating the local atomic stresses [Eq. (4)], we used two different cutoffs. In one case we used the first minimum of the PDF cutoff. In the other case we took into account all atoms within the interaction range. As it could be seen from the figure, there are no significant differences between the self-energies of the pressure component for both of these approaches. The results for shear-stress-energy components are slightly different. The results with the first coordination shell cutoff lie almost exactly on top of the equipartition line. The results with the potential range cutoff lie slightly above the equipartition line. The difference, however, is not significant. It is clear that shear-stress energies also approximately follow the expected equipartition law.

The results for mJp, shown in Fig. 5, are similar to those for the LJ system shown in Fig. 4. We see that the results in a liquid state above ~1500 K again follow the equipartition theorem, as shown earlier.[13] This figure also shows the results from the glassy state at temperatures below 1000 K.

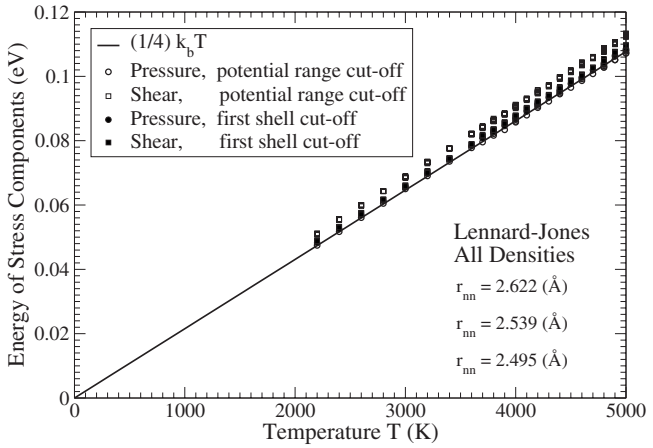

FIG. 4. The stress energies for the systems of particles interacting through shifted Lennard-Jones potential. The figure shows results for all three densities studied. The open squares show energies of all shear components of stress energy calculated using potential range cutoff in Eq. (4). The filled squares show energies of the shear components of the stresses but with a cutoff that corresponds to the first minimum in the pair-density function. The open and filled circles show energies of the pressure component for all densities and two cutoffs (all data are on top of the equipartition line).

The glassy state was obtained by instant temperature drop from the liquid state at 1400 to 800 K, followed by relaxation, and further temperature drops from 800 K to the final temperatures with consequent relaxation. The equipartition rule is obviously violated in the glassy state.[12,13]

Finally the results obtained with the repulsive part of the mJp are presented in Fig. 6. The case of repulsive potential is different from the two previous cases because the range of the potential is short and the system is kept together by the external pressure. Thus the potential is highly asymmetric. Also the cutoff distance is not an issue here (the potential essentially ends at the first maximum of the PDF—not the minimum). In that sense the repulsive potential represents a much more serious challenge to the theory. Nevertheless we see a perfect agreement between the equipartition line and the self-energy of the atomic-level stresses.

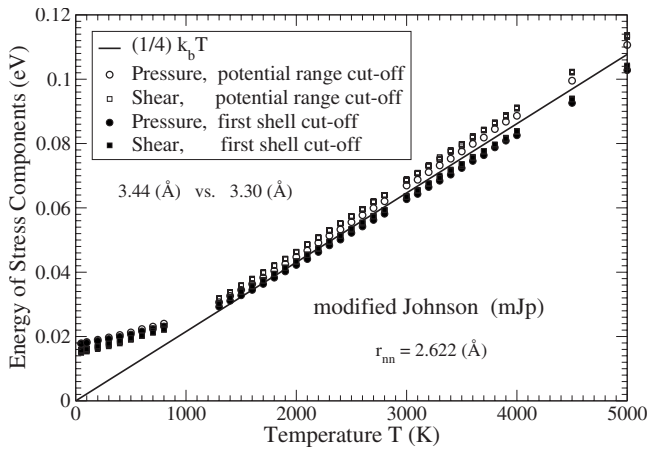

FIG. 5. Similar to Fig. 4 but for the modified Johnson pair potential.

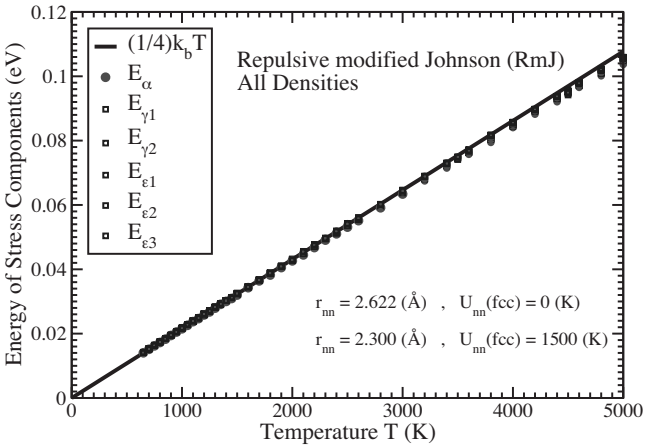

FIG. 6. Similar to Figs. 4 and 5 but for the repulsive part of the modified Johnson potential (results for all seven densities studied are in the figure).

VI. DISCUSSION

The results demonstrate that each component of the self-energy of the atomic-level stresses is not only proportional to temperature but is approximately equal to $(1/4)k_BT$ for various pairwise potentials at various densities. This suggests that the equipartition rule for the stress self-energy is a general feature of the high-temperature liquid. Thus the dynamics of the atomic-level stresses appears to represent the quasinormal modes of the system.

We know that phonons with wavelength much longer than interatomic spacings propagate even in the liquid, and that they are the normal modes of the system at low frequencies. However, the weight of these modes is very small compared to the total density of phonons. In addition, it is shown in Appendix B (in Fig. 9) that some atomic sites have zero or negative values of local shear elastic constants. This implies local softness and instability of atomic position. Strong damping and scattering of phonons by these sites would lead to localization of modes. The localized normal modes can be similar to the "rattlers" mentioned, for example, in Ref. 23. This localization of atomic dynamics must be the reason why the use of the atomic-level stresses as the effective normal modes is justified. At high enough temperatures, the collective dynamics of atoms is sufficiently localized to the nearest-neighbor shell of an atom so that the dynamics of the atomic-level strain becomes the effective normal mode.

Our results have shown that each component of the self-energy of the atomic-level stresses is equal to $(1/4)k_BT$ at high temperatures. However, as shown in Fig. 5, the data deviates from the equipartition line at low temperatures. This is expected since the equipartition line extrapolates to zero at $T=0$, meaning that the stresses have to be zero everywhere at $T=0$. In terms of the atomic-level pressure, for instance, this means that every interatomic distance is equal to the value at the minimum of the pairwise potential, as in the ideal glass structure discussed in deriving Eq. (12). Of course such an ideal structure cannot be reached. Thus, as temperature is lowered, the system would become nonergodic and the self-energy of the stresses would freeze into a nonzero value at a certain temperature.

This logic was used as the basis for the recent theory of glass transition.[20] In this case it was further assumed that the atomic-level stresses are dressed by the long-range stress field,[12] approximately described by the continuum theory of Eshelby.[21] Thus below a certain temperature, above the glass transition temperature,[13] the atomic-level stresses are no longer independent but interact through the long-range stress field. However when the self-energy of the stresses is renormalized with the dressing by the long-range stress field, the equipartition theorem should be recovered.[12] The success of the theory of the glass transition[20] implies that the equipartition law must be valid not only at high temperatures, as demonstrated here, but at all temperatures down to just above the glass transition temperature if the atomic-level stresses are properly renormalized.

VII. CONCLUSION

In this paper we examined the possibility of describing the dynamics of liquids at the atomic level in terms of the quasiharmonic vibrations of the nearest-neighbor shells, represented by the atomic-level stresses. Often the dynamics of liquids is discussed in terms of local-density fluctuations. The atomic-level stress tensor includes the density (pressure) as the trace of the tensor. However, besides the pressure, there are five shear components. Thus the description by the atomic-level stress tensor is more extensive than the description by the fluctuations in the density, a scalar.

One of the main predictions of the mean-field atomic-level stress fluctuation theory is the equipartition of stress self-energies among six different stress components as in Eq. (17). We have carried out the MD simulations to test this equipartition theorem on three distinct pairwise potentials at different densities. We indeed found that the equipartition rule holds with excellent precision in all cases studied. Thus our results show that the equipartition of self-energy of atomic-level stresses between components is a rather general property, i.e., valid for different potentials and densities. The results imply that the quasiharmonic vibrations of the nearest-neighbor shells, represented by the atomic-level stresses, provide a good basis for describing the structure and properties of liquids and glasses.

At present our analysis has been limited to the single-component systems. Since real glasses are usually multicomponent systems, we plan to perform multicomponent simulations in the near future. We also plan to test this approach with an embedded atom many-body potential.[22]

ACKNOWLEDGMENTS

This research has been sponsored by the Division of Materials Sciences and Engineering, Office of Basic Energy Sciences, U.S. Department of Energy under Contract No. DE-AC05-00OR-22725 with UT-Battelle, LLC.

APPENDIX A: DETAILS OF THE PAIR POTENTIALS

The form of the modified Johnson pair potential used in this study is slightly different from the one that was used previously.[17] The minimum allowed distance used in the previous form was 1.9 Å while we found that at temperatures above 3000 K atoms can come closer than 1.9 Å. Thus we had to modify potential at small distances. In our present work, we used the potential that coincides with the form described previously[17] at distances larger than 2.4 Å. For the distances smaller than 2.4 Å, the form of the potential was slightly modified. The full form of the potential is given below (the intervals of distance r are in Å and energy $\phi(r)$ is in eV).

For $[0<r\leq 2.246948]$, the potential has the form

$$\phi(r) = +2.463595(r-2.977441)^4 - 1.396616(r-2.977441)^2.$$

For $[2.246948<r\leq 2.4]$, the potential has the form

$$\phi(r) = -12.900210(r-2.4)^4 - 15.096180(r-2.4)^3 + 1.372738(r-2.4)^2 - 0.504775(r-2.4) - 0.200211.$$

For $[2.4<r\leq 3.0]$, the potential has the form

$$\phi(r) = -0.639230(r-3.115829)^3 + 0.477871(r-3.115829) - 0.092606.$$

For $[3.0<r\leq 3.44]$, the potential has the form

$$\phi(r) = 14.671110(r-3.0)^5 - 12.910630(r-3.0)^4 + 1.725326(r-3.0)^3 + 0.222124(r-3.0)^2 + 0.452143(r-3.0) - 0.146964.$$

The potential, defined in this way, has a continuous second derivative everywhere. The potential has minimum of depth $\phi(r_{\min})=-0.2516$ eV at $r_{\min}=2.6166$ Å.

The corresponding parameters of the cut and shifted Lennard-Jones potential,

$$\phi_{\mathrm{LJ}}(r<2.5\sigma) = 4\epsilon\left[\left(\frac{\sigma}{r}\right)^{12} - \left(\frac{\sigma}{r}\right)^{6}\right] + \delta,$$

are $\sigma=2.3312$ Å, $\epsilon=0.2558$ eV, and $\delta=0.0042$ eV.

APPENDIX B: DISTRIBUTIONS OF PARAMETERS AND THEIR AVERAGE VALUES

In this section we present some results on distributions of parameters that enter into the expressions for the self-energies of atomic-level stresses. The results presented were obtained with the LJ potential at the number density of particles, $\rho=0.07843$ Å^{-3}, that corresponds to the distance, $r_{nn}=2.6223$ Å, between the nearest neighbors in fcc lattice.

Figure 7 shows the distributions of local atomic volumes V_i that were calculated using the following expressions:[8–13]

$$V_i = \left(\frac{4\pi}{3}\right) r_i^3, \quad r_i = \frac{1}{2}\frac{\sum_j w_{ij} r_{ij}}{\sum_j w_{ij}}, \quad w_{ij} = \frac{1}{r_{ij}^2}. \tag{B1}$$

In Eq. (B1) the contribution of the neighbor j to the average radius r_i of the shell around atom i is proportional to the solid angle, Ω_{ij}, which atom j blocks, as seen from atom i,

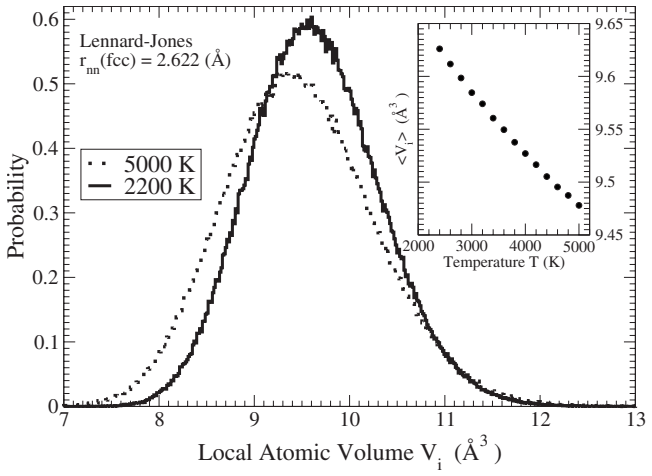

FIG. 7. The main plot shows distributions of the local atomic volume, as defined by Eq. (B1), for the highest studied temperature of 5000 K and the lowest temperature (2400 K) at which liquid does not crystallize for a relatively long time. The cutoff distance was chosen to be $r_{\text{cut-off}}=1.3\cdot 2.62$ Å$=3.41$ Å, which corresponds to the position of the first minimum in the pair distribution function (see Fig. 3). As temperature decreases, the peak position shifts to the right. The inset shows how the average value of local atomic volume depends on temperature.

i.e., $(\Omega_{ij}\propto w_{ij})$. Thus, atoms that are further away from the central atom contribute less to the average radius of the shell than atoms that are closer. In all our calculations the chosen value of cutoff in Eq. (B1) corresponds to the first minimum in the pair-density function.

Figure 8 shows the distributions of stress components σ^{α}

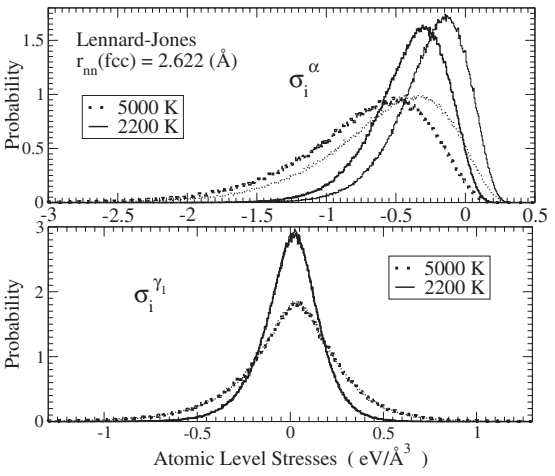

FIG. 8. The distributions of the atomic-level stresses, as defined by Eqs. (4)–(6), at two temperatures. At high temperatures the distributions are wide and they become narrower as temperature is reduced. The thicker lines were obtained with the first coordination shell cutoff in expression for the stresses [Eq. (4)]. The thinner lines were obtained with the potential range cutoff. We see that, for the pressure component of the stresses σ^{α}, the distributions shift to the right as cutoff range increased. The distributions of shear stress σ^{γ_1}, however, do not show any significant changes. The distributions for the other shear stresses are essentially identical to the distributions for σ_{γ_1}.

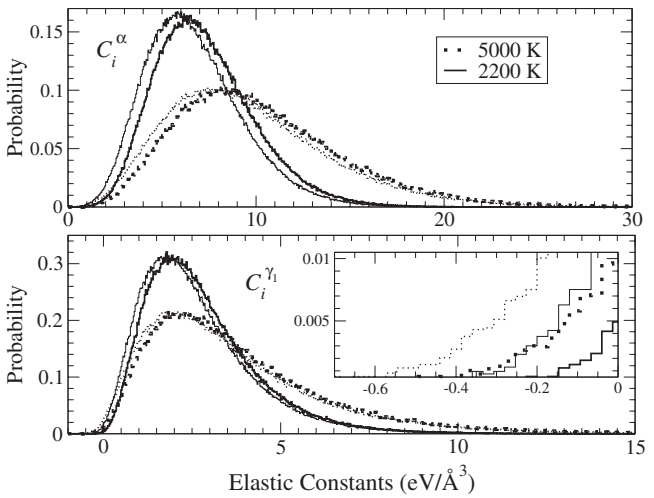

FIG. 9. The main plots show distributions of C_i^{α} (upper) and $C_i^{\gamma_1}$ (lower) elastic constants for two temperatures. The thicker curves are for the first nearest-neighbor cutoff while the thinner curves are for the potential range cutoff. Note that some $C_i^{\gamma_1}$ elastic constants have negative values or have values that are close to zero. Thus the inset in the bottom plot shows on a larger scale the part of the main bottom plot with these negative values for the first coordination shell cutoff.

and σ^{γ_1}. The distributions of other shear-stress components are almost identical to those of σ^{γ_1}, as they should be.

Figure 9 shows the distributions of the local atomic elastic constants C_i^{α} and $C_i^{\gamma_1}$. The distributions for the other shear elastic constants are almost identical to those of $C_i^{\gamma_1}$, as they

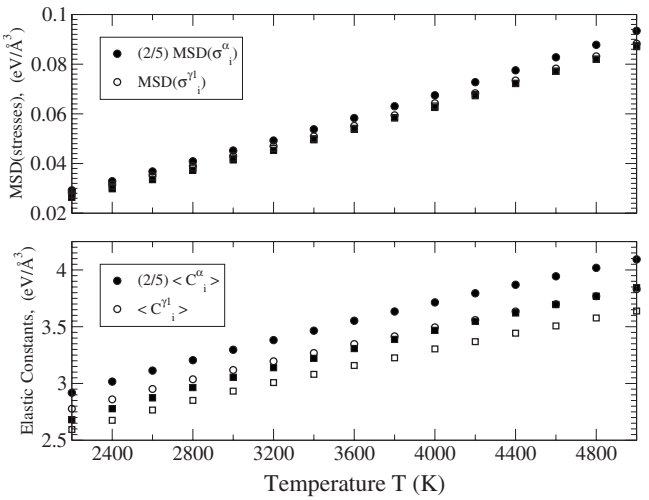

FIG. 10. The upper plot shows temperature dependence of the mean-square deviation of the values of the local atomic stresses. The solid/open circles correspond to the α/γ_1 component with the cutoff corresponding to the first minimum of the PDF. The results for the other shear components are identical to those of γ_1. The results from the potential range cutoff are represented with solid/open squares. The bottom plot shows temperature dependence of the average values of the local atomic elastic constants. The notations are similar to those in the upper plot. The values of elastic constants increase with temperature because the volume was kept constant.

should be. It could be seen in Fig. 9 that some sites have zero or negative values of local shear elastic constants. Thus the atomic configurations involving these sites are unstable with respect to some deformations, as discussed in Sec. VI of the paper.

Note that the larger (potential range) cutoff for the pressure component of the stress shifts the distribution to the right. This behavior is expected since one can obtain the following expression for the σ_i^α from Eqs. (4) and (5),

$$\sigma_i^\alpha = \frac{1}{2\sqrt{3}}\left(\frac{1}{V_i}\right)\sum_j \left[\frac{d\phi(r_{ij})}{dr_{ij}}\right] r_{ij}. \tag{B2}$$

When we consider potential range cutoff, we include the second (and third) coordination shells into account. The derivatives for the second and third neighbors in Eq. (B2) are positive. Thus the distribution and average pressure shift to the right.

A similar argument works for the elastic constant C_i^α, which is given by

$$C_i^\alpha = \frac{1}{6}\left(\frac{1}{V_i}\right)\sum_j \left[\frac{d^2\phi(r_{ij})}{dr_{ij}}\right] r_{ij}^2. \tag{B3}$$

For the second and third nearest neighbors, the second derivative is negative. Thus the inclusion of the second and third nearest neighbors shifts the distribution to the left.

However, the shifts in the distributions of stresses and elastic constants do not affect the values of the stress energies in a significant way. Thus for the pressure component shown in Fig. 4, there is almost no difference. On the other hand, while we essentially do not see much differences between the distributions of shear stresses for the two cutoffs, we do see small changes (due to elastic constants) in the values of the energies for the shear-stress components (Fig. 4).

The upper plot in Fig. 10 shows the temperature dependence of the mean-square deviations of local atomic stresses. The bottom plot shows the temperature dependence of the average values of local atomic elastic constants. The values of elastic constants increase with temperature because the volume was kept constant.

[1] Y. Rosenfeld and P. Tarazona, Mol. Phys. **95**, 141 (1998).
[2] Y. Gebremichael, M. Vogel, M. N. J. Bergroth, F. W. Starr, and S. C. Glotzer, J. Phys. Chem. B **109**, 15068 (2005).
[3] F. H. Stillinger and T. A. Weber, Science **225**, 983 (1984).
[4] P. G. Debenedetti, *Metastable Liquids: Concepts and Principles* (Princeton University Press, Princeton, NJ, 1996).
[5] P. G. Debenedetti and F. H. Stillinger, Nature (London) **410**, 259 (2001).
[6] R. Zwanzig, Phys. Rev. **156**, 190 (1967).
[7] T. Keyes, J. Phys. Chem. **101**, 2921 (1997).
[8] T. Egami, K. Maeda, D. Srolovitz, and V. Vitek, J. Phys. (Paris), Colloq. **41**, C8 (1980).
[9] T. Egami, K. Maeda, and V. Vitek, Philos. Mag. A **41**, 883 (1980).
[10] D. Srolovitz, K. Maeda, V. Vitek, and T. Egami, Philos. Mag. A **44**, 847 (1981).
[11] D. Srolovitz, T. Egami, and V. Vitek, Phys. Rev. B **24**, 6936 (1981).
[12] T. Egami and D. Srolovitz, J. Phys. F: Met. Phys. **12**, 2141 (1982).
[13] S.-P. Chen, T. Egami, and V. Vitek, Phys. Rev. B **37**, 2440 (1988).
[14] J. D. Weeks, D. Chandler, and H. C. Andersen, J. Chem. Phys. **54**, 5237 (1971).
[15] M. P. Allen and D. J. Tildesley, *Computer Simulation of Liquids* (Clarendon, Oxford, 1987).
[16] R. A. Johnson, Phys. Rev. **134**, A1329 (1964).
[17] T. Tomida and T. Egami, Phys. Rev. B **52**, 3290 (1995).
[18] L. V. Woodcock, Chem. Phys. Lett. **10**, 257 (1971).
[19] D. M. Heyes, *The Liquid State: Applications of Molecular Simulations*, Tutorial Series in Theoretical Chemistry (Wiley, New York, 1998).
[20] T. Egami, S. J. Poon, Z. Zhang, and V. Keppens, Phys. Rev. B **76**, 024203 (2007).
[21] J. D. Eshelby, Proc. R. Soc. London, Ser. A **241**, 376 (1957).
[22] J. R. Morris, R. S. Aga, V. A. Levashov, and T. Egami, Phys. Rev. B **77**, 174201 (2008).
[23] C. S. O'Hern, L. E. Silbert, A. J. Liu, and S. R. Nagel, Phys. Rev. E **68**, 011306 (2003).